https://doi.org/10.5194/egusphere-2024-1200
Preprint. Discussion started: 14 May 2024

Diurnal variation of amplified canopy urban heat island in Beijing megacity during heat wave periods: Roles of mountain-valley circulation and urban morphology

Tao Shi[1], Yuanjian Yang[2*], Ping Qi[1], Simone Lolli[3]

[1]School of Mathematics and Computer Science, Tongling University, Tongling, 244000, China
[2]School of Atmospheric Physics, Nanjing University of Information Science and Technology, Nanjing, 210044, China
[3]CNR-IMAA, Contrada S. Loja, 85050 Tito Scalo (PZ), Italy

Correspondence to: Prof. Yuanjian Yang (yyj1985@nuist.edu.cn)

Abstract. In the context of global warming and rapid urbanization, heat waves (HW) are becoming more frequent, which is amplifying canopy urban heat island (CUHI) via various driving mechanisms. While the roles of local circulation and urban morphology remain unclear in the synergistic interaction between HW and CUHI. By utilizing the data from high-density automatic weather stations in the Beijing megacity, this article explored spatiotemporal patterns of the interactions between HW and CUHI. The average daily CUHII during HW periods exhibited a significant increase of 59.33% compared to the non-heat wave (NHW) periods. Mountain-valley breeze significantly modulated the spatiotemporal patterns of CUHI intensity (CUHII). In particular, on an urban scale, the turning mountain-valley breeze caused horizontal transport of heat inner-city, resulting in the north-south asymmetric pattern of urban excess warming during HW periods. On a street scale, the amplified CHUII was closely associated with urban morphology in the inner city, especially for the vertical characteristics of buildings. During the mountain breeze phase, the amplification of CUHII in the high-rise street zone was significantly stronger than that in the low-rise street zone. During the valley breeze phase, the amplification of CUHII in high-rise street zones exhibits weaker effects in the afternoon compared to the low-rise street areas, while demonstrating stronger amplification during the nighttime. Our findings provide scientific insight to understand the driving mechanisms of urban excess warming and mitigating the escalating risks associated with extreme high-temperature events over megacities in the transitional zone of mountains and plains.

1 Introduction

The interaction between climate and urbanization and their potential synergistic effects hasbecome one of the key topics of in current global climate change research (Seto et al., 2012; Ding, 2018), e.g, the interaction between increased heat wave (HW) and enhanced canopy urban heat island (CUHI) (Li & Bou-Zeid, 2013; Founda et al., 2015; Khan et al., 2020; Ngarambe et al., 2020; Zinzi et al., 2020). Even during the hiatus of global warming, the frequency and duration of HW events also exhibited an increasing trend worldwide, posing significant challenges to the urban thermal environment and the resultant public health (IPCC,2023; Patz et al., 2005; Xu et al., 2016; Yang et al., 2017). With the acceleration of

https://doi.org/10.5194/egusphere-2024-1200
Preprint. Discussion started: 14 May 2024

urbanization and population aggregation, the CUHI in megacities has become increasingly prominent (Liu et al., 2007; Zheng et al., 2018; Yang et al., 2020), exacerbating the occurrence of regional extreme high temperature events (Zong et al., 2021), and seriously affecting urban development and the health of residents (Gao et al., 2015; Jiang et al., 2019). For instance, compared to non-heat wave (NHW) periods, the average CUHII in Shanghai has increased by 128.91% during HW periods (Yang et al., 2023), while the maximum CUHII in Seoul can increase by 4.5°C during HW periods (Ngarambe et al., 2020). The rate of contribution of urbanization to the excessive mortality caused by high temperatures can reach more than 45% in the high-density urban areas (Zong et al., 2022). Therefore, in the context of global warming and rapid urbanization, it is very important to explore various driving mechanisms for urban excess warming caused by the interaction between HW and CUHI at different time scales.

In terms of natural impact factors, the uneven temporal and spatial distribution of urban excess warming is significantly affected by local circulation in different geographical environments (Zhang et al., 2011; Zhou et al., 2020; Chen et al., 2022). Few studies focused on the impact of local circulations on the amplified CUHII during HW periods (Yang et al., 2023; Xue et al., 2023). The strong sea breeze transports cold and wet sea air to the urban area, which can weaken the CUHII and decrease the frequency of occurrence of HW events during daytime in Shanghai (Yang et al., 2023). During HW periods, the mountain-valley breeze enhanced the vertical turbulent heat transfer, and improved ventilation conditions reduced aerosol concentration (the urban canopy received more short-wave radiation), both of which are beneficial to the enhancement of CUHII in Lanzhou (Xue et al., 2023). Overall, the current understanding of the mechanisms through which local circulations modulated the amplified CUHII during HW periods is still in the exploratory stage.

From the perspective of anthropogenic impact factors, urban morphology is also an important factor influencing the local thermal environment (Oke, 2006; Merckx et al., 2018; Tian et al., 2019). Building height has a complex impact on solar radiation during daytime and long-wave radiation at night (Srivanit & Kazunori, 2011; Oke et al., 2017), while building density alters the wind field in open spaces (Erell et al., 2011; Ao et al., 2019). Local Climate Zones (LCZs) define the range of values for parameters such as land cover, average building height, and sky view factor (SVF) within a climate zone, enabling the discovery of the characteristics of thermal environmental variations within cities (Stewart & Oke, 2012; 2014). Scholars have studied the urban excess warming in different LCZs, advancing the quantitative research on the synergies between HW and CUHI (Ngarambe et al., 2020; Zheng et al., 2022; Xue et al., 2023; Yang et al., 2023). The intensity, frequency, and duration of HW events in LCZ1 and LCZ2, which are dominated by dense mid-rise and high-rise buildings, are significantly stronger than in other types of climate zone (Yang et al., 2023). However, LCZs are a comprehensive indicator of urban morphology, and the aforementioned studies have not quantified the contribution of different urban morphological parameters to the local thermal environment, nor have they taken into account the nonlinear driving effects of urban morphology on the local thermal environment (Alonso & Renard, 2020; Chen et al., 2022).

Currently, it is still matter of debate the roles of local circulations and urban morphology in amplifying CUHI in megacities during HW periods. The main objective of this study is considering as case study the megacity of Beijing, using high-density automatic weather stations (AWS) observations. By combining remote sensing data and the machine learning method, this

https://doi.org/10.5194/egusphere-2024-1200
Preprint. Discussion started: 14 May 2024

research article analyzed the synergies mechanisms between HW and CUHI, aiming to provide technical support for high-temperature forecasting, the improvement of living environments, as well as urban planning and management.

2 Data and methodology

2.1 Study Area

In 2022, Beijing's population had exceeded 20 million and the built area was more than 1,400 km2, making it one of the most urbanized cities in China. The terrain of Beijing is exceptionally complex, northly bounded by Yan Mountains by Taihang Mountains in the west. The altitudes of those mountains exceede 2,000 meters. The northeastern part comprises hilly terrain, while the southern region is dominated by plains. The area extending from the east to the southeast is a zone where land and sea intersect, bordering Bohai Bay. Under conditions of weak weather systems, the mountain-valley breeze formed by the complex terrain plays a dominant role in the atmospheric circulation of the Beijing area (Liu et al., 2009; Miao et al., 2013; Dou et al., 2014).

https://doi.org/10.5194/egusphere-2024-1200
Preprint. Discussion started: 14 May 2024

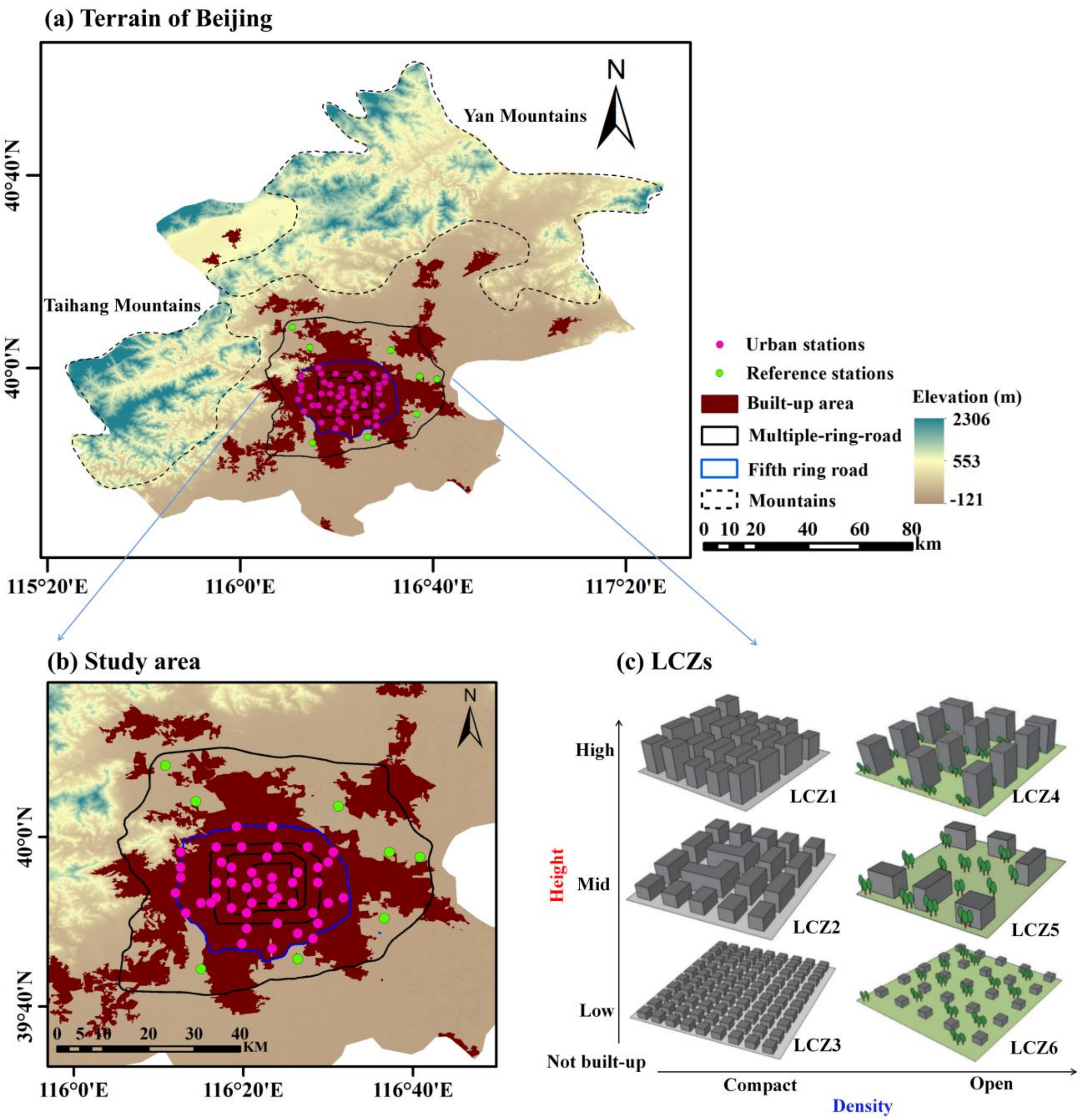

Figure 1: Overview of study area. (a) Terrain and land use of Beijing. (b) Study area map. (c) Empirical examples of the typical LCZ types.

80 ## 2.2 Data

2.2.1 Urban morphology datasets

Land cover modulates the energy exchange, water, and carbon cycle between different regions of the Earth, and accurate land cover data is the basic parameter of climate research. In the past few decades, the land cover in China has greatly

https://doi.org/10.5194/egusphere-2024-1200
Preprint. Discussion started: 14 May 2024

changed with the development of the economy. The annual China Land Cover Dataset (CLCD) is a dynamic data set accounting for land use in China released by Professor Yang and Professor Huang of Wuhan University. Yang & Huang (2021) made the land cover datasets with a spatial resolution of 30 m based on 335,709 Landsat images on Google Earth Engine. The latest datasets contain information on China's land cover from 1985 to 2021, and the overall precision of land classification is 80%. The LCZ datasets in this article were provided by the Institute of Urban Meteorology, China Meteorological Administration. The building skyline and floor data of the electronic map were extracted using Python language. The height of each floor was estimated to be 3 m, to obtain information on the height of the buildings within the research buffer areas of the target stations.

2.2.2 AWS observation data

The hourly AWS observation data used in this article were obtained from the China Meteorological Data Service Center (http://data.cma.cn/en), which primarily encompasses near-surface air temperature, wind speed, wind direction and other related elements. To ensure the rigor of the data, we conducted quality control on the observed meteorological data at ground stations. Following previous methods (Yang et al., 2011; Xu et al., 2013), missing values in observation sequences were replaced with the average of synchronous observation data from the five nearest stations surrounding the given station, and stations with excessive error records were excluded. Consequently, 53 stations evenly distributed throughout the study area were selected for a detailed analysis of the spatio-temporal characteristics of the near-surface thermodynamic field in Beijing.

2.3 Methods

2.3.1 Definition of HW and CUHII

In this study, the HW events were selected based on a relative threshold of the daily maximum temperature. Specifically, a weather process in which the daily maximum temperature exceeds the 90th percentile threshold of the temperature climatology and persists for three days or longer is considered a daytime HW event (Russo et al., 2014). Drawing from observations recorded at all stations in Beijing between June 1 and August 31, from 2016 to 2020, it was determined that the 90^{th} percentile of the daily maximum temperature is 35°C. Days with precipitation (specifically, daily precipitation exceeding 0.1 mm) and days with typhoon were excluded, as per previous studies (Du et al., 2017; Walsh & Chapman, 1998). If 30% or more of the stations within a day experience HW events, that day was defined as an HW day; otherwise, it was considered an NHW day.

Other researches calculated the CUHII by selecting reference stations for ground temperature observations and urban stations (Ren et al., 2007; Shi et al., 2015). This study identified stations that were less influenced by the urban effect and located outside of a 50km radius from the city center, based on the spatial distribution characteristics of near-surface temperature. Additionally, the stations must have a rural environment and be evenly distributed in different directions throughout the city. According to these criteria, eight reference stations were selected, with an average altitude of 39.6m, which is only 8.8m lower than the average altitude of 45 urban stations (Fig. 1). The amplified CUHII was obtained by subtracting the CUHII during the NHW periods from the CUHII during the HW periods.

https://doi.org/10.5194/egusphere-2024-1200
Preprint. Discussion started: 14 May 2024

2.3.2 Calculation of mountain-valley breeze

In the Beijing region, the most significant local circulation is the valley breeze. During the day, the wind blows from the valley to the mountain due to the thermal difference between the valley and its surrounding air, while at night, the wind reverses direction, blowing from the mountain to the valley (Tian & Miao, 2019). However, local circulation can be difficult to observe as a result of the influence of mesoscale weather patterns. Therefore, when analyzing valley breezes, it is crucial to remove the effects of mesoscale wind field. According to the method used by Cao et al. (2015) and Zheng et al. (2018), this article decomposed the wind measurements at each station into components u (east-west direction) and v (north-south direction), calculated their average values and considered them as the actual wind. By averaging the hourly data, the daily average wind U and V were obtained, which were regarded as the background wind. Finally, this paper subtracted the background wind from the actual wind to obtain the local circulation wind.

2.3.3 Indicators of urban morphology

Numerous horizontal parameters (2D) and vertical parameters (3D) have been used to quantify urban morphology (Zakšek et al., 2011; Tompalski & Wężyk, 2012; Berger et al. 2017). Here, we selected six indicators of horizontal morphology and six indicators of vertical morphology to measure the morphological characteristics around AWS (Table 1). Horizontal indicators represent the physical properties of the underlying surface and were used to explore the effect of the underlying surface on the air temperature. Vertical indicators reflect the complex effect of landscape pattern on wind field and solar radiation within neighborhoods. The calculation of horizontal and vertical urban morphology indicators was based on land cover datasets and building height information.

Table 1: Summary of the spatial morphological parameters.

Indicators	Description
2D	
BCR	Building cover ratio, which represents the proportion of the roof of the building to that of the entire study area.
NEAR	Mean distance between adjacent buildings.
NP	Number of patches.
SPLIT	Splitting index, which represents the degree of separation of landscape segmentation. The greater the value, the more fragmented the landscape.
AI	Aggregation index, which represents the connectivity between patches of each type of landscape. The smaller the value, the more discrete the landscape
L/W	Building length-width ratio.

https://doi.org/10.5194/egusphere-2024-1200
Preprint. Discussion started: 14 May 2024

3D	
H	The height of buildings, which represents the average height of all buildings in the buffer zone.
H-max	Maximum height of buildings in the study area.
H-std	The standard deviation of building height in the study area.
FAR	Floor area ratio, which represents the ratio of the sum of gross floor area to total study area.
CI	Cubic index, which represents the ratio of the building volume to the total study volume.
SVF	Sky view factor, which represents the ratio of radiation received by a planar surface from the sky to that received from the entire hemispheric radiating environment.

2.3.4 Fitting model

Multiple linear regression analysis is a statistical method to determine the quantitative relationship between dependent variables and multiple independent variables (Li, 2020). Although the traditional linear regression model is straightforward and intuitive, it frequently falls short in effectively addressing intricate non-linear relationships. Support Vector Regression (SVR) is widely used as an effective supervised learning method. By introducing the concept of support vectors, SVR improves the fitting ability of data while maintaining the complexity of the model (Smola & Schölkopf, 2004). The Random Forest (RF) model, a popular and highly flexible machine learning approach (Breiman, 2001), can simulate complex nonlinear relationships between predictive values and diverse predictors (Hastie et al., 2009). The RF model exhibits low sensitivity to outliers and missing values in data sets, and, because of the law of large numbers, it is less prone to overfitting. Previous studies have shown that the RF model is effective in fitting complex problems and measuring the importance of factors (Tan et al., 2017; Yu et al., 2020).

Taking amplified CHUII as the dependent variable, the influencing factors were input into the linear model, the SVR model, and the RF model including 2D indicators and 3D indicators as independent variables. The impact of urban spatial morphology on urbanization bias was evaluated based on the importance scores and significance of the input parameters to the model. The construction of various models, the importance scores of the influencing factors and the significance testing were implemented using Python code.

https://doi.org/10.5194/egusphere-2024-1200
Preprint. Discussion started: 14 May 2024

3 Results

3.1 The spatial-temporal pattern of urban excess warming

The vast urban expansion has led to a constant increase in urban population density, while human activities have generated significant anthropogenic heat and pollutant emissions, thereby amplifying urban excess warming to a certain extent.

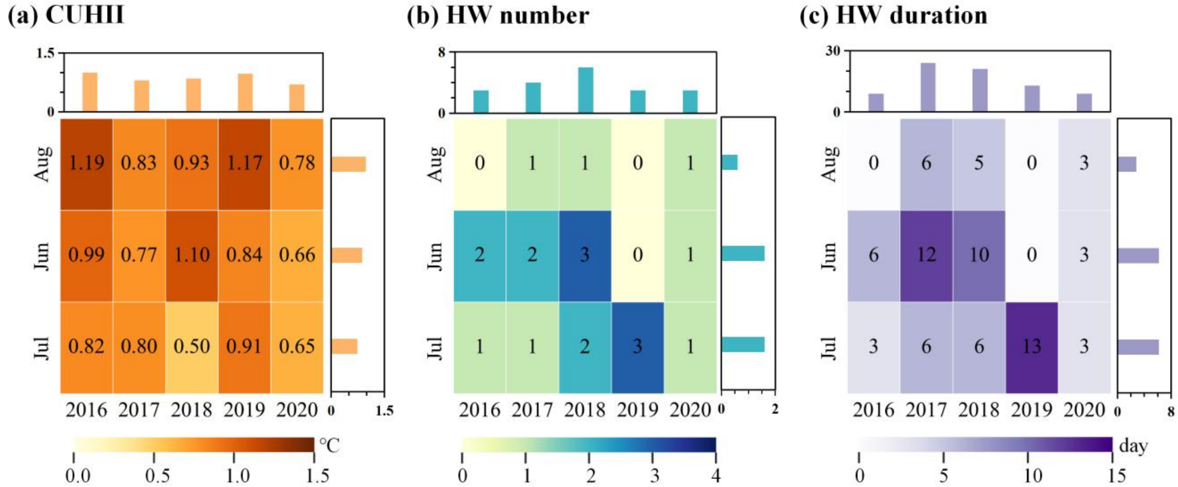

Figure: 2 The temporal variations of urban excess warming from 2016 to 2020. (a) CUHII, (b) number of HW events, and (c) duration of HW events.

Fig. 2 illustrates significant inter-annual variations in urban excess warming in Beijing. Specifically, 2016 and 2020 were years with relatively weaker urban excess warming, with three occurrences and a total duration of nine days. Conversely, 2017 and 2018 exhibited stronger urban excess warming, with four and six occurrences, and a total duration of 24 and 21 days. The occurrence and persistence of such widespread high-temperature events in the North China region are closely related to specific atmospheric circulation anomalies. Potential influencing factors include the circulation pattern of the 500 hPa geopotential height field (Sun et al., 2011), ocean-atmosphere anomalies such as changes in the cold and warm phases in the equatorial central and eastern Pacific, as well as the position and intensity of the warm high-pressure ridge over the continent or the subtropical high over the northwest Pacific (Wei & Sun, 2007). Furthermore, there are distinct intraseasonal variations in CHUII and HW events in Beijing. HW events are stronger in June and July, averaging 6.2 days per month, significantly higher than in August. Intraseasonal variations in urban excess warming may be associated with combined differences in weather conditions, including precipitation, wind vectors, cloud cover, fog, and air pollution (Unger et al., 2001; He BJ, 2018; Chen et al., 2022).

https://doi.org/10.5194/egusphere-2024-1200
Preprint. Discussion started: 14 May 2024

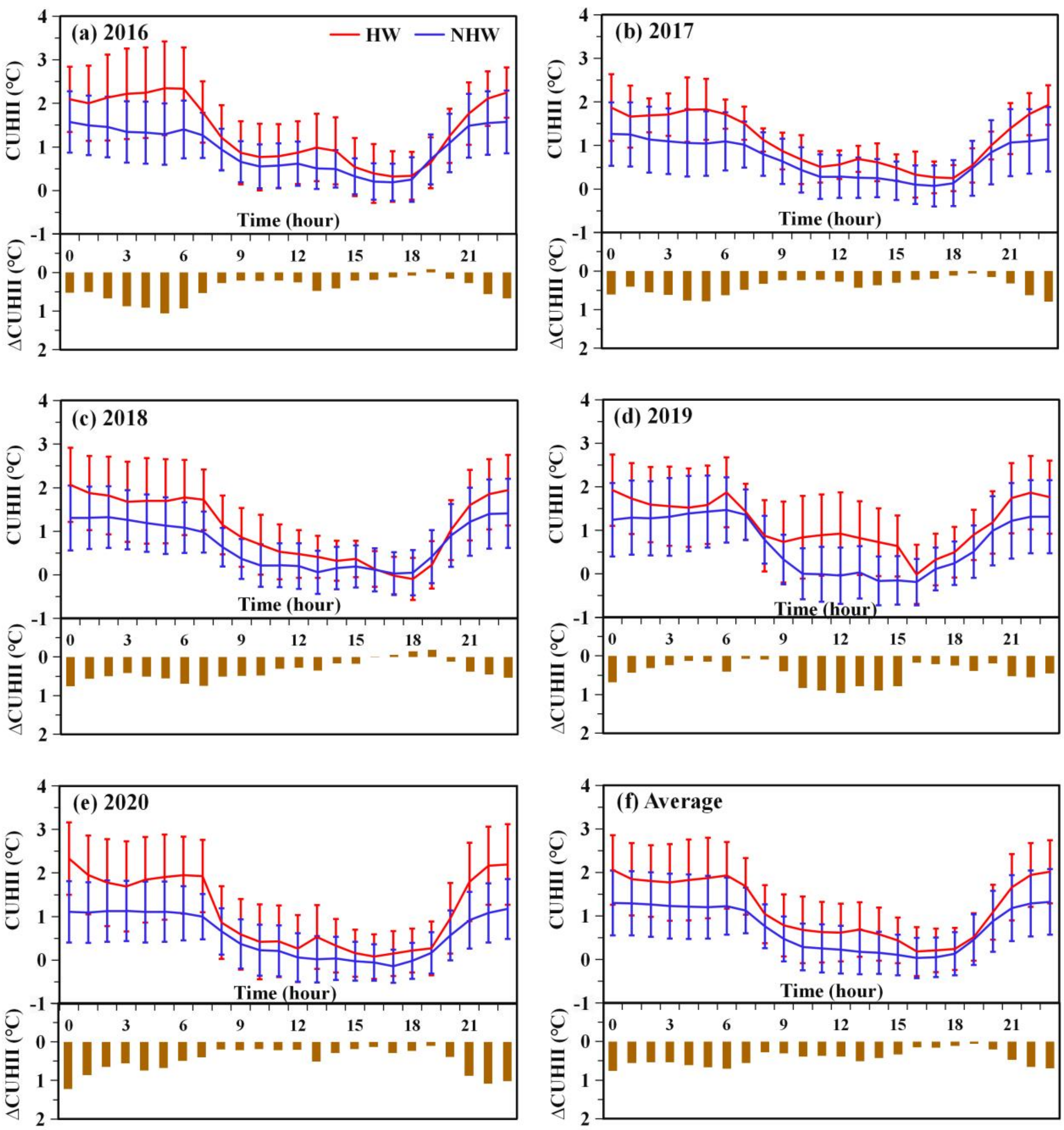

Figure: 3 Diurnal variation (Beijing time, BJT) and standard deviation of CUHII during HW and NHW periods in the built-up area of Beijing. (a) 2016, (b) 2017, (c) 2018, (d) 2019, (e) 2020, (f) mean value from 2016 to 2020.

Fig. 3 describes that the daily variation of the CUHII in Beijing during summer shows a U-shaped fluctuation. The peak of CUHII typically occurs in the early morning and remains relatively stable throughout the entire night. The CUHII in built-up areas of Beijing exhibited more fluctuation during the daytime. The CUHII began to decrease significantly at 06:00 BJT and reached its lowest point at 16:00 BJT. During HW periods, the CUHII range was between 0.18 and 2.06℃, while during NHW periods, it varied between 0.03 and 1.32℃. In particular, the average daily CUHII during the HW periods exhibited a

https://doi.org/10.5194/egusphere-2024-1200
Preprint. Discussion started: 14 May 2024

significant increase of 59.33% compared to the NHW periods. The diurnal variation of CUHII may be modulated by anthropogenic heat emissions, aerosols, atmospheric circulation, etc. (Zheng et al., 2018; Zheng et al., 2020; Yang et al., 2020). The maximum amplified CUHII (ΔCUHII) was 0.76℃, occurring at midnight, while the minimum ΔCUHII was 0.05℃, observed at 19:00 BJT. It should be noted that the ΔCUHII remained positive throughout the daytime and nighttime, indicating the persistent synergies between HW and CUHI in the built-up area of Beijing.

https://doi.org/10.5194/egusphere-2024-1200
Preprint. Discussion started: 14 May 2024

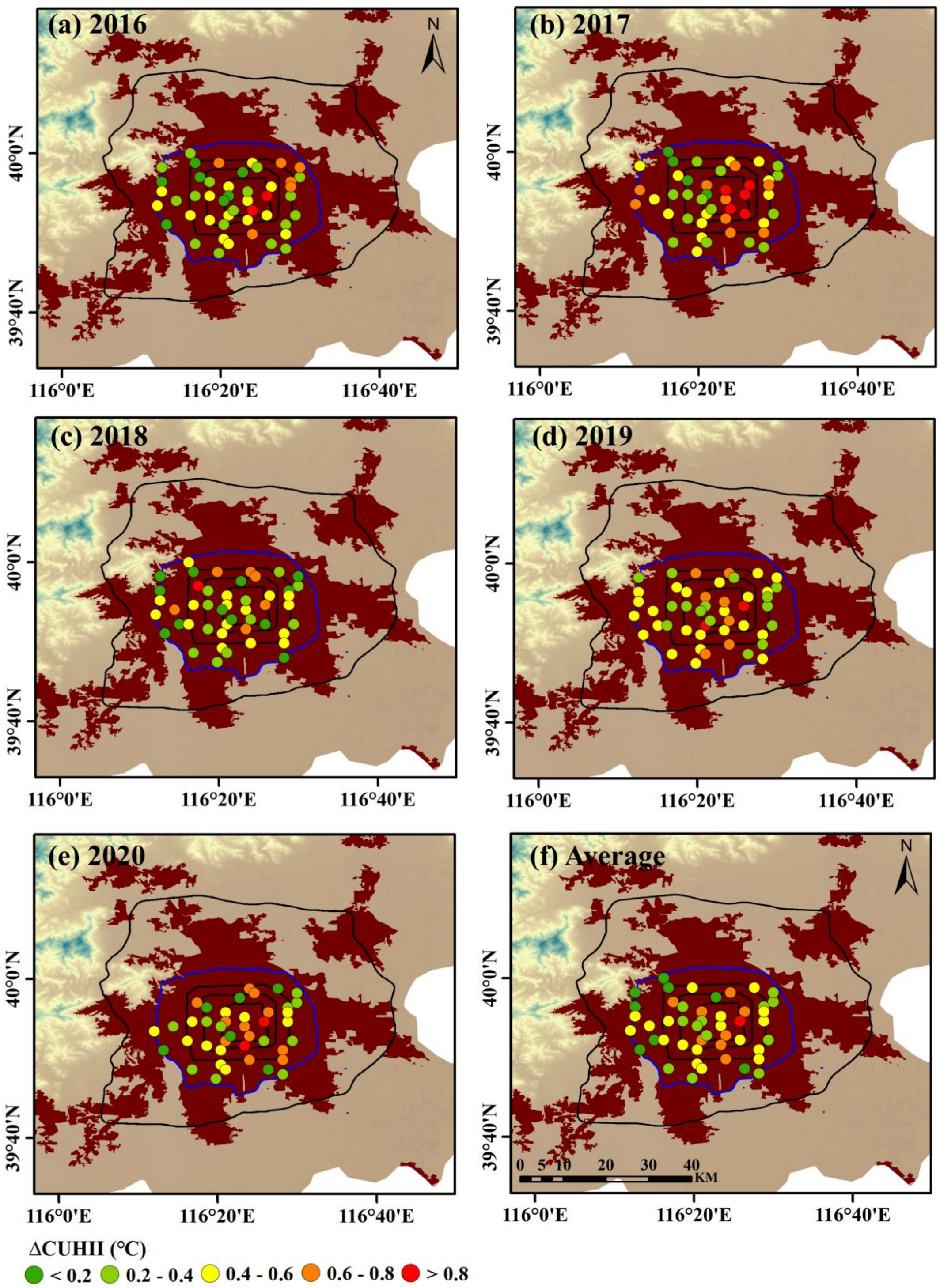

190

Figure: 4 Spatial patterns of amplified CUHII (ΔCUHII) during HW periods. (a) 2016; (b) 2017; (c) 2018; (d) 2019; (e) 2020; (f) average value from 2016 to 2020.

https://doi.org/10.5194/egusphere-2024-1200
Preprint. Discussion started: 14 May 2024

Fig. 4 illustrates that the synergies between HW and CUHII were strongest in 2017, with amplified CUHII exceeding 0.8℃ at six stations in the urban center. Conversely, the weakest synergies occurred in 2018, with only one station in the urban center recording an amplified CUHII above 0.8℃. Significant spatial variations were observed in the distribution of amplified CUHII. Taking the average amplified CHUII as an example (Fig. 4f), the minimum amplified CUHII values were distributed at the edges of the urban area, while the maximum values were located between the Second and Fourth Rings in the urban center. During HW periods, the urban surface receives more short-wave and long-wave radiation, increasing heat storage (Zong et al., 2021), leading to a stronger CUHII during HW periods (Zheng et al., 2018), leading to excess urban warming (Fenner et al., 2019; He et al., 2021).

3.2 Modulation of amplified CHUII by local circulation

Local circulations caused by different geographical environments have a significant impact on the spatial and temporal distribution of urban extreme high temperatures (Zhang et al., 2011; Zhou et al., 2020; Chen et al., 2022). The western and northern parts of Beijing are surrounded by mountains, and the mountain-valley breeze strongly impacts the thermal dynamic field near-surface of Beijing megacity (Miao et al., 2013; Dou et al., 2014). In this section, this research analyzed the modulation of mountain-valley breeze on the synergies between HW and CUHI using wind field and temperature data from AWS.

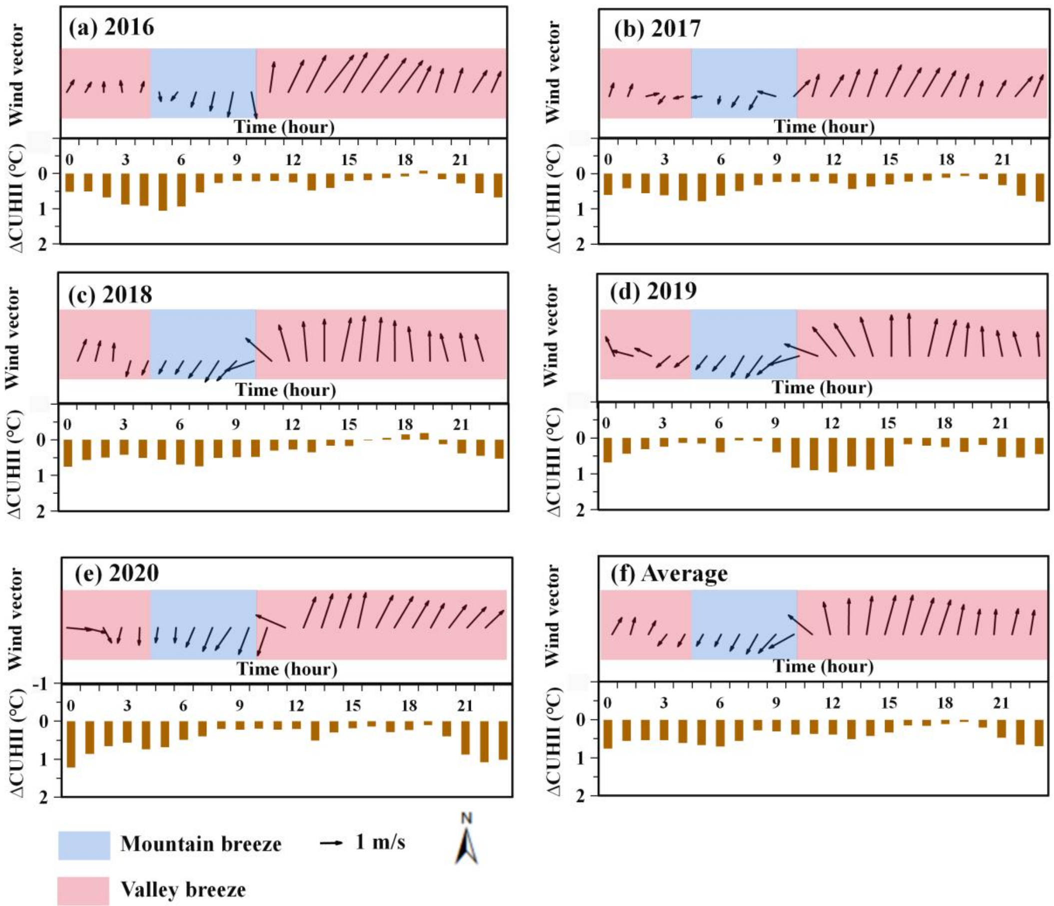

Figure: 5 Diurnal variations (Beijing time, BJT) in wind direction, wind speed, and amplified CUHII in the built-up area of Beijing during HW periods. (a)2016, (b)2017, (c)2018, (d)2019, (e)2020, (f) average value from 2016 to 2020.

As depicted in Fig. 5, the urban area was dominated by northerly winds from 05:00 BJT to 10:00 BJT, with a notable reversal in wind direction occurring at 11:00 BJT, resulting in south winds dominating the urban area until 04:00 BJT of the following day. This phenomenon indicates the significant presence of mountain-valley breeze in Beijing during summer. In 2017, the wind speeds were the lowest, with average mountain breeze and valley breeze speeds of 0.63m/s and 1.24m/s, respectively. Conversely, 2019 saw the highest wind speeds, with average mountain breeze and valley breeze speeds of 0.91m/s and 1.59m/s, respectively. Overall, the mountain breeze persisted for approximately 5 hours with an average wind speed of 0.95m/s, while the valley breeze lasted for approximately 19hours with an average wind speed of 1.21m/s. The speed of the mountain breeze was significantly lower than that of the valley breeze, consistent with previous studies (Dou et al., 2014). Furthermore, the average amplified CHUII during the mountain breeze phase (0.49℃) was higher than that during the valley breeze phase (0.41℃), potentially related to the variable wind speed during different stages of mountain-valley circulation.

https://doi.org/10.5194/egusphere-2024-1200
Preprint. Discussion started: 14 May 2024

This study analyzed the spatial distribution characteristics of amplified CHUII in the urban north (UN) and urban south (US) (as shown by the black dashed line in Figs. 6c-d). The effectiveness of urban natural ventilation hinges on the exchange and flow of air within the urban canopy, which has a direct impact on the high temperature environment within cities (Yang et al., 2023). Figs. 6a-b illustrates that, regardless of whether it is the mountain breeze phase or the valley breeze phase, the correlations between wind speed and amplified CUHII were both negative. Except for the mountain breeze period in the urban south, the other p-values were lower than 0.1. In the future, we plan to expand our research area to encompass the Beijing-Tianjin-Hebei urban agglomeration. Low wind speeds typically result in poorer urban ventilation environments (Ng, 2009; Bady et al., 2011), especially in areas with densely packed urban buildings that hinder the flow of cold air. With reduced airflow and limited heat dispersion under weak wind conditions, these conditions further exacerbate urban excess warming (Gemechu et al., 2022).

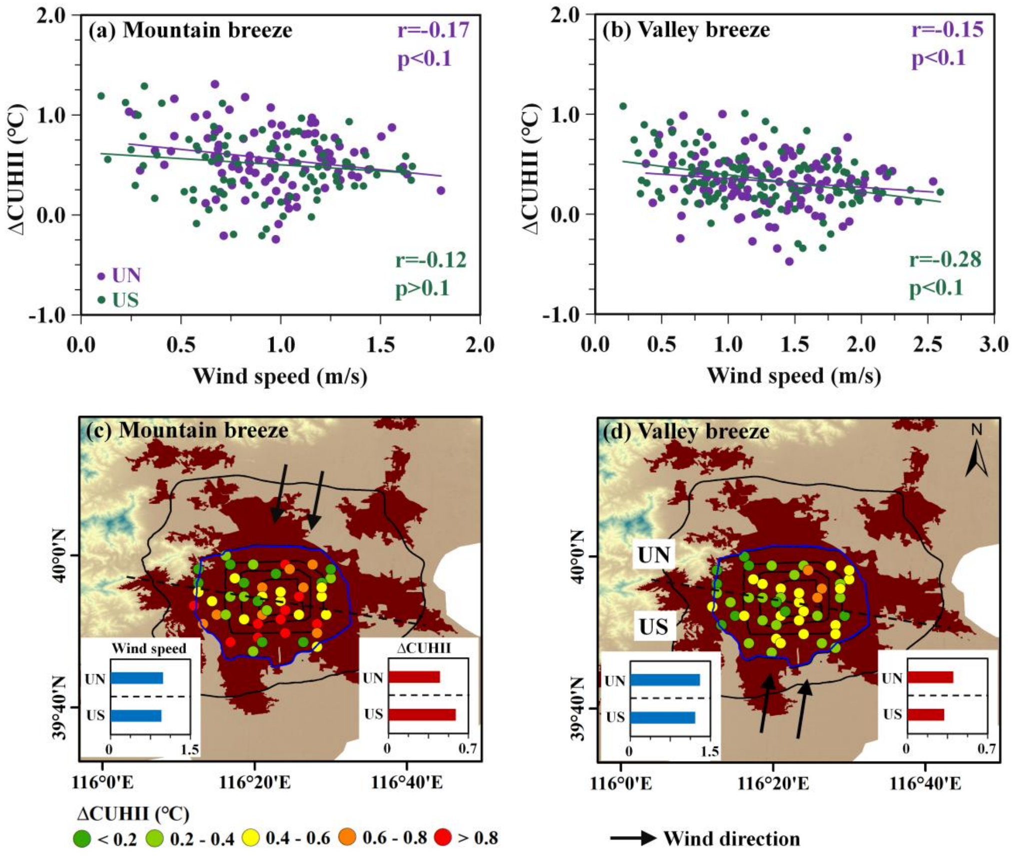

Figure: 6 Correlation analysis between wind speed and amplified CUHII at various stations from 2016 to 2020 during the mountain breeze phase (a) and the valley breeze phase (b). The spatial patterns of amplified CUHII during the mountain breeze phase (c) and valley breeze phase (d).

https://doi.org/10.5194/egusphere-2024-1200
Preprint. Discussion started: 14 May 2024

During the mountain breeze phase, the wind direction is from north to south (as indicated by the black arrow in Fig. 6c). As shown in Fig. S1, in the urban north, the year with the highest average amplified CUHII was 2016 (0.55℃), while the lowest average occurred in 2019 (0.41℃). In contrast, the urban south experienced its maximum amplified CUHII in 2020 (0.59℃) and its lowest in 2017 (0.51℃). Despite the slightly higher average wind speed in the southern part (0.89 m/s) compared to the northern part (0.88 m/s), the annual average amplified CUHII in the southern part (0.57℃) was significantly higher than that in the northern part (0.48℃). During this phase, the wind blows from south to north (as indicated by the black arrow in Fig. 6d). In Fig. S2, the year with the highest average amplified CUHII in the urban north was 2017 (0.47℃), while the lowest was 2018 (0.35℃). In the urban south, the maximum average amplified CUHII occurred in 2020 (0.38℃), and the minimum was in 2018 (0.21℃). Although the average wind speed in the urban north (1.30 m/s) was higher than that in the urban south (1.22 m/s), the annual average amplified CUHII in the urban north (0.40℃) was significantly higher than that in the urban south (0.32℃). On an urban scale, it was evident that wind speed might not be the primary regulatory factor for urban excess warming.

Wind speed was inversely proportional to amplified CUHII at individual stations, indicating that good ventilation conditions could improve the thermal environment around individual locations. However, for the entire city, a more consistent wind field at the ground level results in a stronger heat transport capacity (Xie et al., 2022; Yang et al., 2023). Taking the valley breeze as an example, under its influence, the heat from the southern part of the city was horizontally transported to the northern part, exacerbating urban excess warming in the northern areas. Therefore, on an urban scale, the turning mountain-valley breeze caused horizontal transport of heat inner city, resulting in the north-south asymmetrical pattern of urban excess warming during HW periods.

3.3 Response of amplified CUHII to urban morphology

On a street scale, the spatial heterogeneity of urban areas and their infrastructure can directly contribute to the spatially inhomogeneous distribution of the near-surface air temperature (Fenner et al., 2017). In this section, we further explored the causes of the synergies of HW and CHUII in Beijing, focusing on urban morphology.

https://doi.org/10.5194/egusphere-2024-1200
Preprint. Discussion started: 14 May 2024

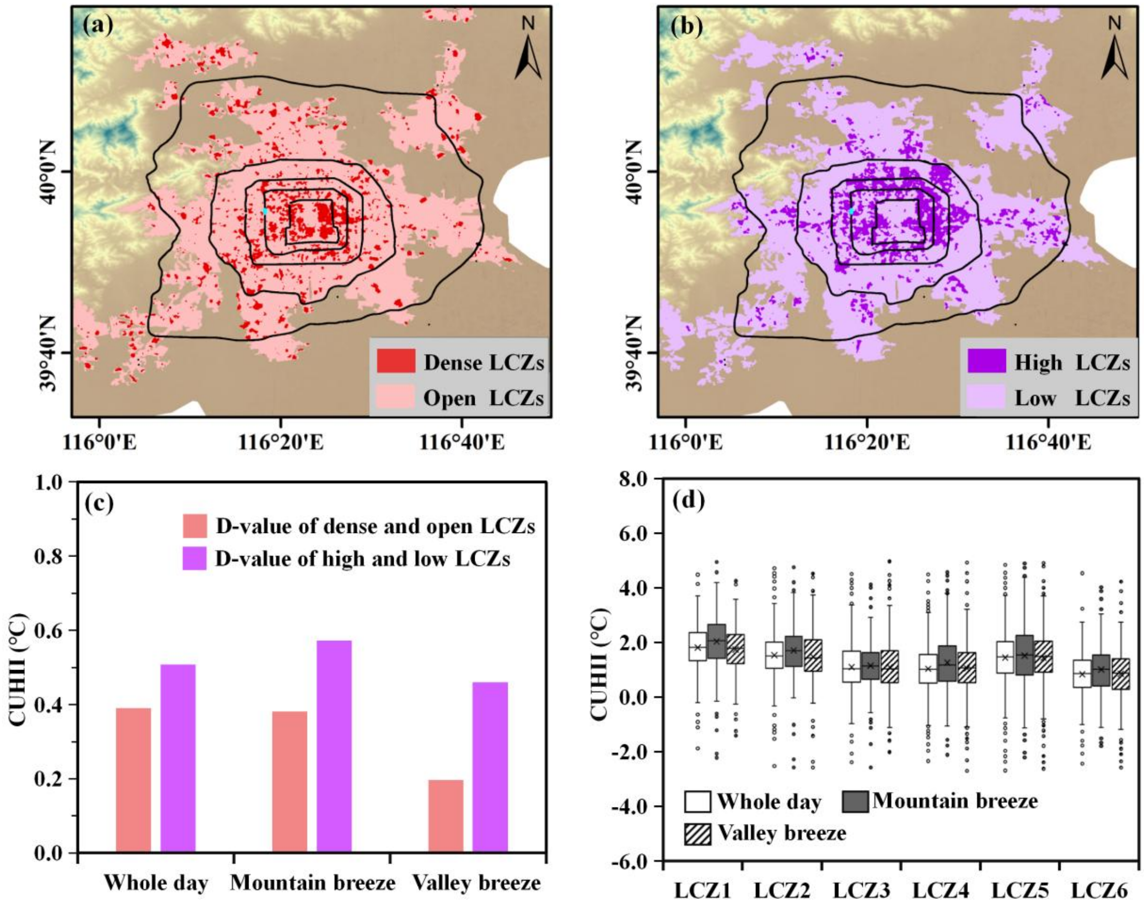

Figure: 7 (a) Urban configuration structures dominated by density information, including dense buildings (LCZ1, LCZ2, LCZ3) and open buildings (LCZ4, LCZ5, LCZ6). (b) Urban configuration structures are dominated by height information, including high-rise buildings (LCZ1, LCZ2, LCZ4, LCZ5) and low-rise buildings (LCZ3, LCZ6). (c) Difference value (D-value) in CUHII across different urban configuration structures. (d) Box-and-whisker plots comparing the CUHII values for various LCZs.

From the perspective of urban configuration structures (Figs. 7a-b), dense buildings were mainly concentrated within the Second Ring Road of the built-up area, while high-rise buildings were primarily distributed between the Second and Fourth Ring Roads. Notably, most of the stations with high urban excess warming were located in areas with high-rise buildings. Fig. 7c demonstrates that the D-value in CUHII between dense and open LCZs ranges from 0.20-0.39°C, while the D-value between high and low LCZs was 0.46-0.57°C. Previous studies have shown that in densely populated high-rise building areas of Beijing, HW events occur more frequently and last longer (Zong et al., 2021). Similar results are obtained in this study. Among the various LCZs, LCZ1, characterized by dense high-rise buildings, exhibits the highest mean CUHII value of 1.71°C for the built-up area of Beijing. The average CUHII for LCZ2, LCZ3, LCZ4, LCZ5, and LCZ6 is 1.43, 0.98, 0.91,

https://doi.org/10.5194/egusphere-2024-1200
Preprint. Discussion started: 14 May 2024

1.34, and 0.71℃, respectively (Fig. 7d). Therefore, apart from local circulation patterns, the CUHII was also dependent on the characteristics of the urban underlying surface.

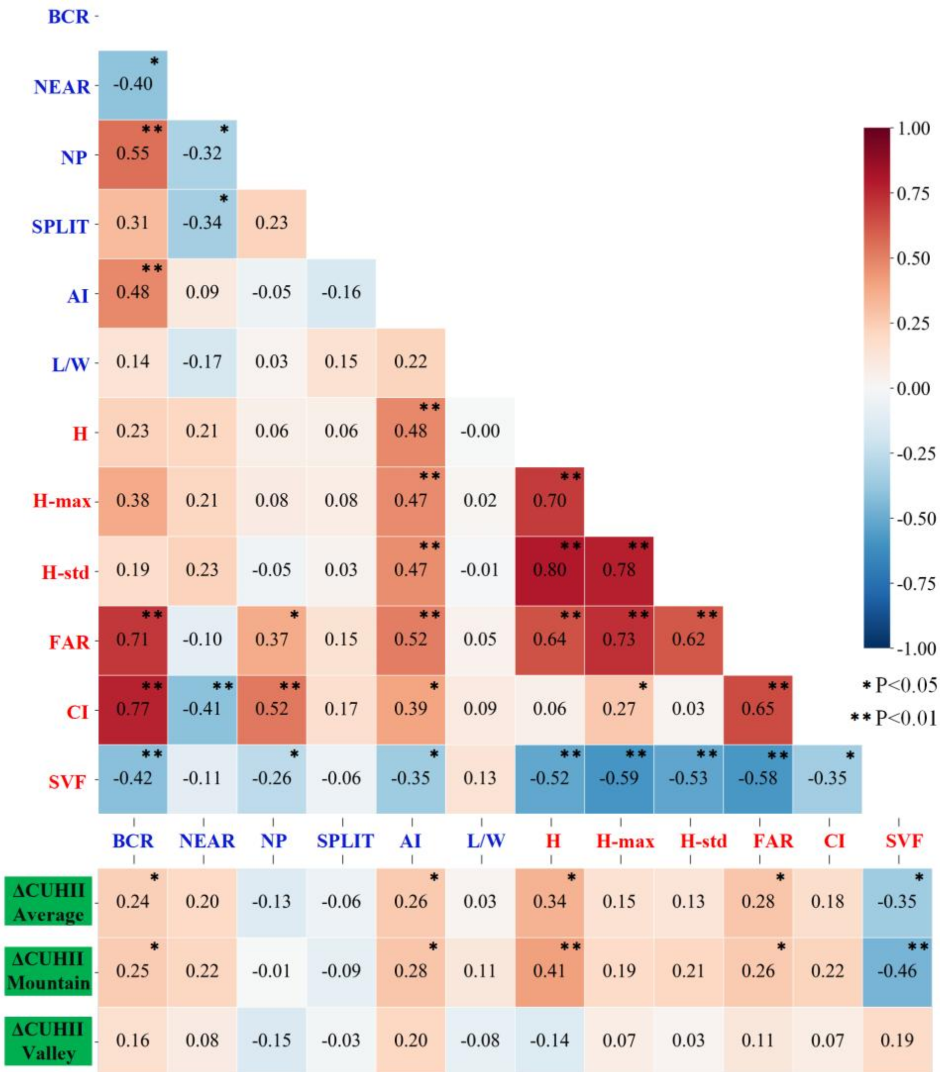

Figure: 8 Spearman rank correlation coefficients between indicators of urban morphology and amplified CHUII during different local circulation periods. The blue characters represented the 2D urban morphological parameters, while the red characters represented the 3D urban morphological parameters.

The Spearman correlation analysis showed that the associations between 3D morphological indicators and amplified CHUII were generally higher than those of 2D indicators (Fig. 8). Indicators using a combination of morphological aspects generally had stronger correlations with temperature (Tian et al., 2019). For example, SVF had the highest correlations with amplified CHUII during 3D indicators. The correlation between the floor area ratio (FAR) and the amplified CHUII was

https://doi.org/10.5194/egusphere-2024-1200
Preprint. Discussion started: 14 May 2024

stronger than the building cover ratio (BCR). In addition, the strength of the correlation between 2D and 3D indicators and amplified CHUII varied greatly during different local circulation periods. Urban morphological indicators had weaker
290 relationships with amplified CHUII during the mountain breeze period but showed stronger correlations with amplified CHUII during the valley breeze period.

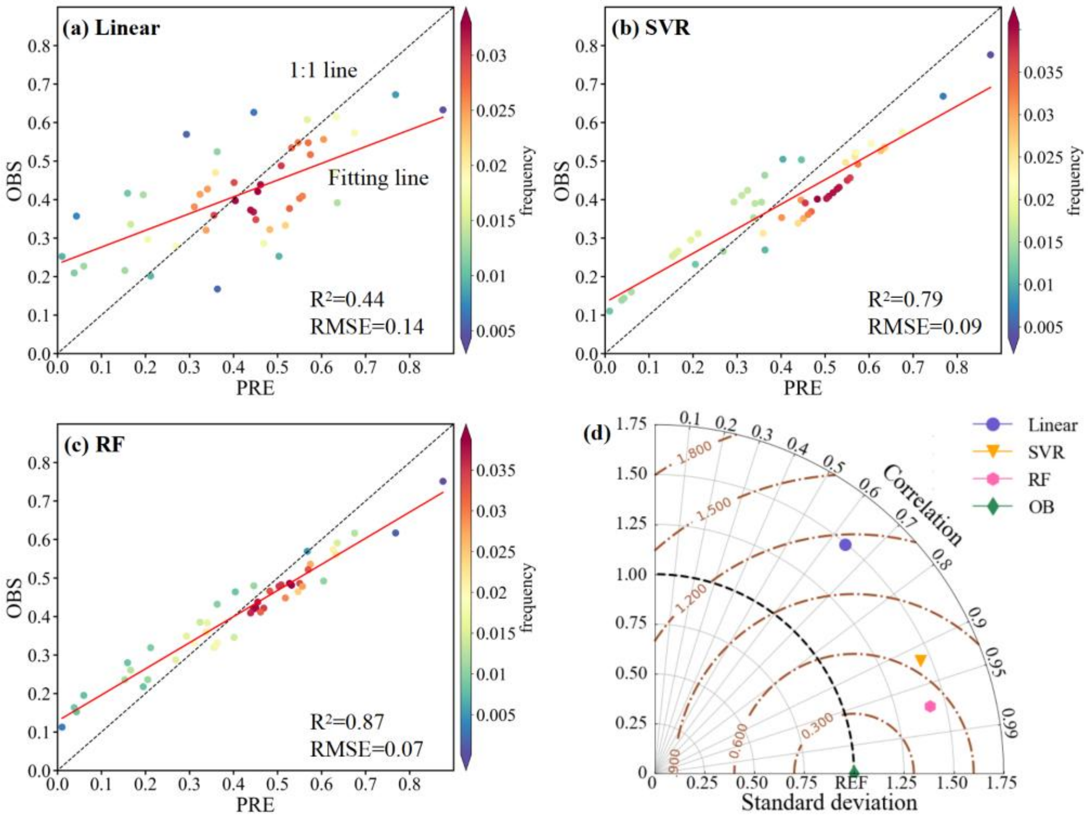

Figure: 9 Comparing the simulation accuracy across different models. (a) Linear model, (b) SVR model, (c) RF model, and (d) Taylor diagrams for various models, where the gray line represents the correlation between the simulated and observed values,
295 **and the brown dashed line indicates the root mean square error between the simulated and observed data.**

The linear model has shown considerable strength in predicting the ΔCHUII with a coefficient of determination (R^2) of 0.44 and root mean square error (RMSE) of 0.14℃ (Fig. 9a). Fig. 9b illustrated that the SVR model demonstrated superior performance compared to the linear model in predicting amplified CHUII, achieving an R^2 value of 0.79 and an RSME value
300 of 0.09℃. Moreover, the RF model was used to explain the contribution of each feature to the prediction of amplified CHUII. Based on the performance values given in Fig. 9c, it appeared that RF had the highest R^2 value of 0.87 and the lowest RMSE value of 0.07℃, which indicated that it had the lowest prediction error and was potentially more accurate than other models. In Fig. 9d, the gray ray in the Tylor diagram indicates that the correlation between the data from the linear model and the observed data was relatively low. Additionally, the variation in the linear model data was significantly greater than the

https://doi.org/10.5194/egusphere-2024-1200
Preprint. Discussion started: 14 May 2024

observed variation (indicated by the excessive distance from the origin). In both cases, this results in a relatively large, centered root mean square error (yellow contour line) for the linear model. These results suggest that the performance of the linear model was relatively poor. The RF data were 87% correlated to the real data, while the linear and SVR data had a weaker correlation with the real data. The good performance of RF could be proved by its strong correlation with the real data set. Therefore, the RF model could be considered a reliable tool for fitting the relationship between ΔCHUII and urban morphology.

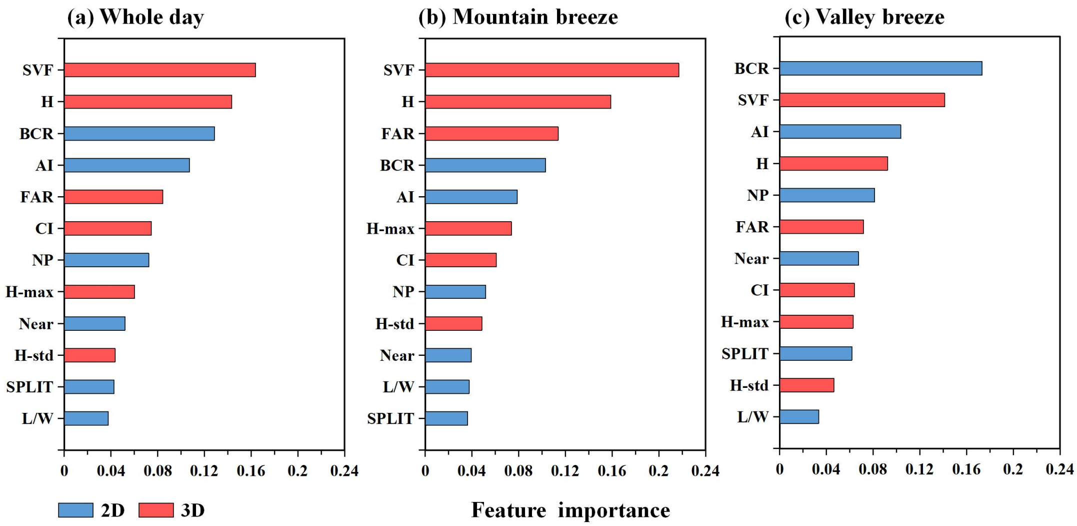

Figure: 10 The importance rank of urban morphological variables for the RF model estimating the ΔCHUII. (a) Whole day, (b) mountain breeze phase, (c) valley breeze phase.

This paper constructed a RF model to compare the relative importance of urban morphology in predicting ΔCHUII. The importance of predictors varied by different local circulations. Throughout the whole day (Fig. 10a), the relative importance method, the following criteria were listed in descending order of importance: SVF, FAR, H, BCR, CI, AI, NP, H-max, Near, H-std, SPLIT, L/W. During the mountain breeze period (Fig. 10b), the order of importance of other indicators changed significantly. Interestingly, in the whole day and mountain breeze period, the SVF was still the most important morphology indicator for predicting ΔCHUII. Previous studies have shown that SVF is closely related to urban LST (Peng et al., 2017; Scarano & Mancini, 2017) and air temperature (Rafiee et al., 2016; Drach et al., 2018). Compared to the immediately neighboring rural area, SVF played a more important influence on determining the land surface temperature in the high-rise built-up area (Jia et al., 2023). During the valley breeze period (Fig. 10c), the importance of SVF to ΔCHUII has weakened, ranking second in the importance list. Building height and SVF had weaker relationships with average daytime temperature but showed stronger correlations with average nighttime temperature (Tian et al., 2019). Overall, the importance list showed that the effects of 3D morphological indicators were stronger than those of 2D indicators on ΔCHUII.

https://doi.org/10.5194/egusphere-2024-1200
Preprint. Discussion started: 14 May 2024

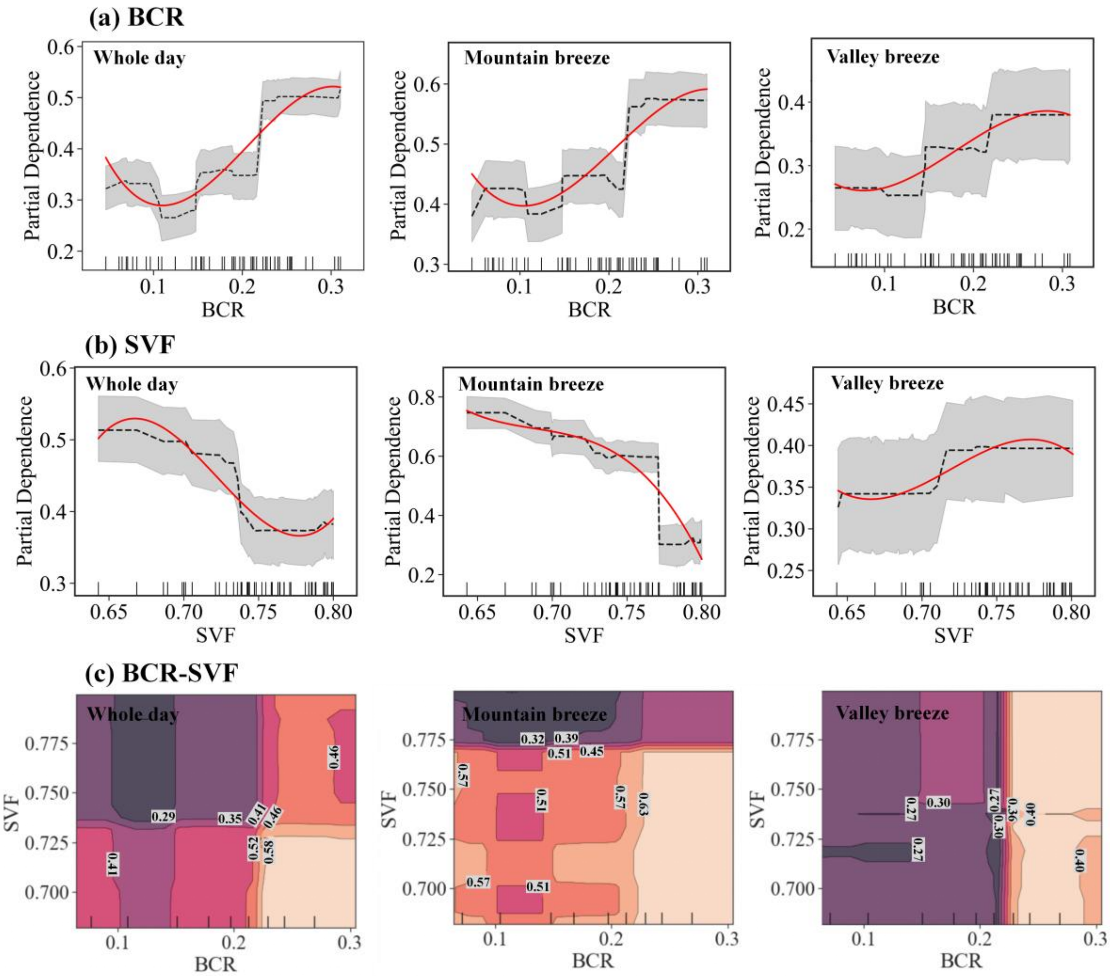

Figure: 11 (a-b) Partial dependence plots of ΔCUHII on BCR and SVF. The red line represents the fitted curve, while the gray lines indicate the 95% confidence interval. (c)The two-way partial dependence plot of ΔCUHII on BCR and SVF.

As the previous text demonstrated, the importance of SVF and BCR in the 2D and 3D indicators was the highest. In Fig. 11a, it could be seen that as the proportion of buildings increased in summer, the ΔCHUII showed a continuous upward trend overall. During the mountain breeze phase, the growth trend of ΔCHUII was higher than that of the entire day and the valley breeze phase. When the BCR exceeded 0.18, the dependence of ΔCHUII on the BCR increased rapidly. There might be a threshold for the building area, and when this threshold was exceeded, the promoting effect of the building area on the urban heat island was significantly enhanced. This complex pattern of association is closely related to urban climatic conditions, vegetation coverage in built-up areas, the frequency of human activities, and seasonal and spatial differences in energy consumption (Guo et al., 2016; Yang et al., 2018; Zhou et al., 2014). In Fig. 11b, during both the whole day and the mountain breeze phase, as SVF increased in summer, the overall synergistic effect exhibited a continuous downward trend.

https://doi.org/10.5194/egusphere-2024-1200
Preprint. Discussion started: 14 May 2024

However, during the valley breeze phase, the dependence increased with increasing SVF, indicating that SVF had an inhibitory effect on ΔCHUII. In addition, the two-way partial dependence plots were constructed to explore the joint effect of two dominant factors (Fig. 11c). The interactions between BCR and SVF relied on their relative values. During the whole day and mountain breeze period, the highest dependence of ΔCHUII occurred in the areas with BCR exceeding 0.2 and SVF less than 0.72. During the valley breeze period, the regions with the highest dependence of ΔCHUII required the presence of SVF greater than 0.75. It could be seen that SVF had a dual impact on ΔCHUII. On one hand, a smaller SVF can increase the absorption of solar radiation by the ground surface (Unger, 2004), making it difficult for heat to dissipate from the streets (Wang, 2009). However, on the other hand, the shading provided by buildings with a low SVF can reduce the surface radiative temperature (Emmanuel, 2010; Perini & Magliocco, 2014).

4 Discussions

Local circulations and urban morphology played pivotal roles in influencing the synergies between HW and CUHI. In the following, this article selected representative stations with typical geographic locations and spatial characteristics of buildings to analyze how local circulations and urban morphology alter the synergies between HW and CUHI.

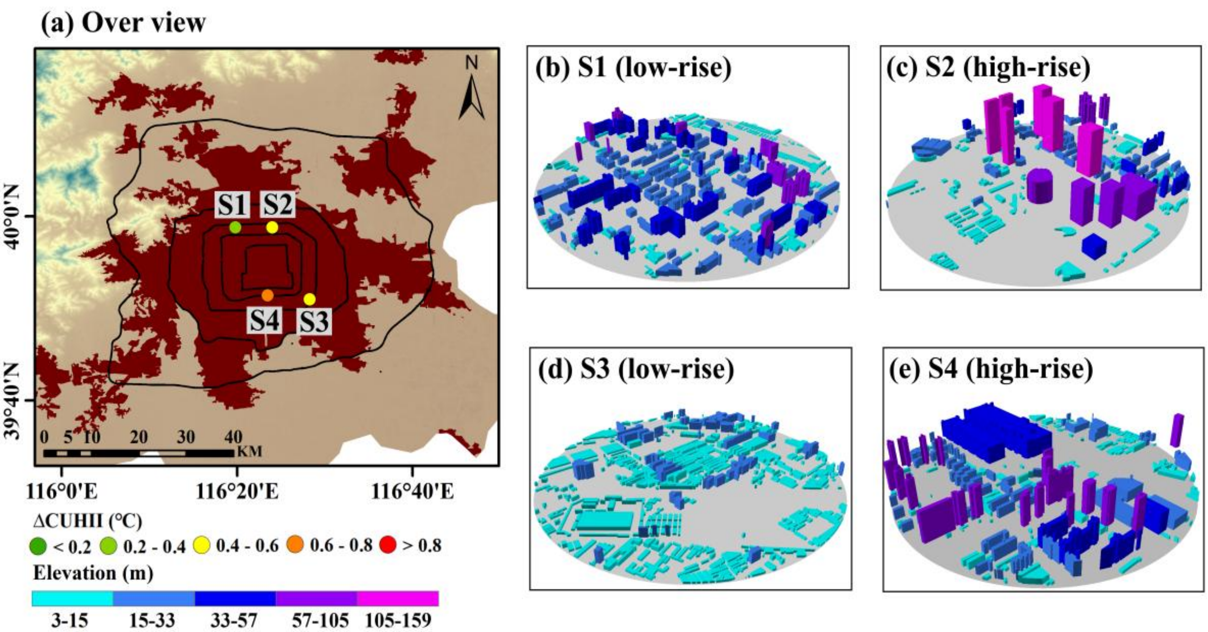

Figure: 12 (a) An overview of representative stations in the built-up area of Beijing. (b-e)Urban morphology around the representative stations.

Taking into account the influence of the mountain-valley breeze, representative stations were selected in the southern and northern parts of the city in this section. Additionally, based on the driving effects of urban morphology, we select high-rise

https://doi.org/10.5194/egusphere-2024-1200
Preprint. Discussion started: 14 May 2024

and low-rise as the criterion. Ultimately, 651061 (S1), 651007 (S2), 651009 (S3), and 651047 (S4) were chosen as representative stations (Fig. 12). S1 and S2 were located between the Third and Fourth Northern Rings, with S1 mainly surrounded by low-rise and S2 dominated by high-rise. Meanwhile, S3 and S4 were situated between the Third and Fourth Southern Rings, with S3 being characterized by high-rise and S4 surrounded by low-rise. The comparison between S1 and S3, as well as the contrast between S2 and S4, could be utilized to investigate the impact of local circulations on the synergistic effect. Additionally, the comparison of S1 with S2, as well as the contrast between S3 and S4 allowed for the analysis of the impacts of urban morphology on synergistic interaction.

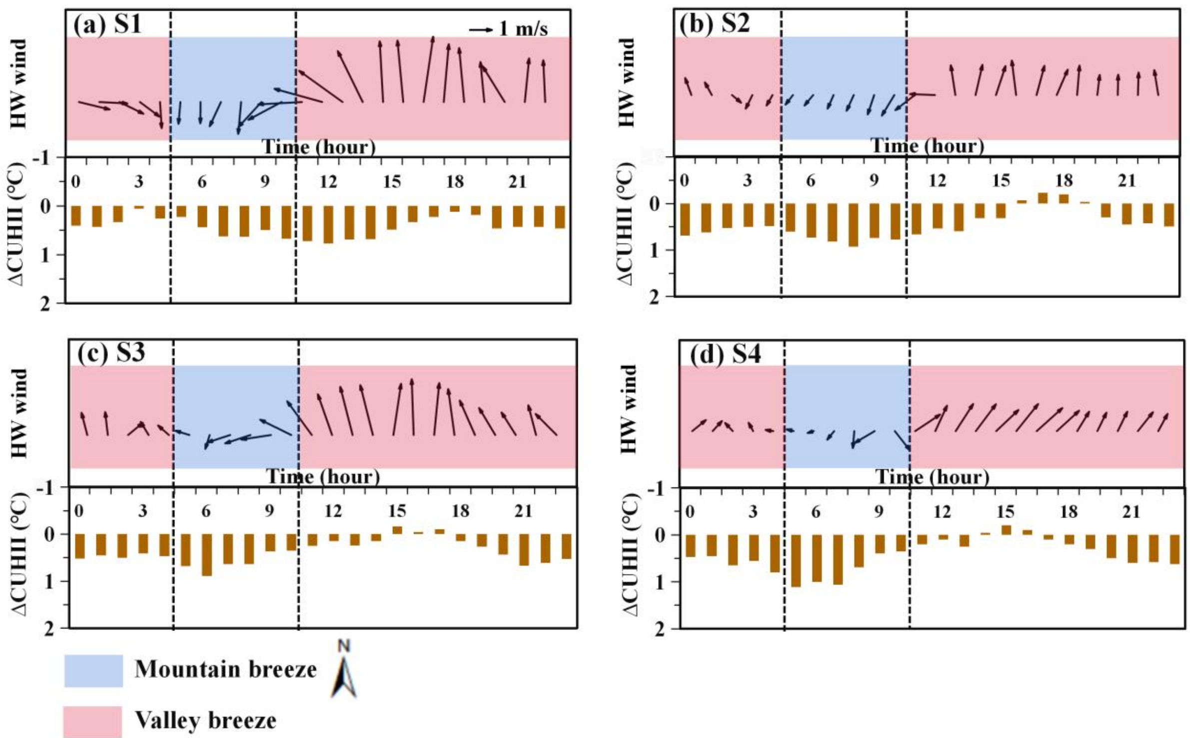

Figure: 13 Diurnal variations in wind direction, wind speed, and amplified CUHII in the built-up area of Beijing during HW periods.

During the mountain breeze phase, the wind direction is from north to south. As depicted in Fig. 13, under the influence of large-scale horizontal heat transport, the synergistic effect observed at S1 (0.51°C) and S2 (0.76°C) located in the northern region was lower than that observed at S3 (0.59°C) and S4 (0.77°C) situated in the southern. Taking the stations in the north as examples, the synergies were more pronounced at S2, surrounded primarily by high-rise neighborhoods, in comparison to S1, which was encircled by low-rise residential areas. Higher CHUII in high-rise neighborhoods is likely due to a combination of more heat being released, less or slower heat dispersion, and lower wind speeds. High-rise residential buildings are associated with higher population densities with greater capacities to mitigate heat, translating to more air conditioners which when operating release additional heat (Ryu & Baik, 2012). High-rise neighborhoods have smaller SVF and thus have less outgoing long-wave radiation (Unger, 2004). Additionally, high-rise neighborhoods tend to experience lower wind speeds (Hang et al., 2011). Wind speed at S1 (1.13 m/s) was significantly greater than that at S2 (0.67 m/s). The lower wind speed at S2 limited the loss of sensible heat through atmospheric convection and advection, making it difficult for heat to dissipate from the streets (Wang et al., 2009). Consequently, the turning mountain breeze phase and the large-scale horizontal transport led to a lower degree of urban excess warming in the northern city compared to the southern city. Moreover, on a street scale, the amplification of CUHII in high-rise street zones was significantly stronger than that in low-rise street zones.

During the valley breeze phase, the wind direction is from south to north. Under the influence of large-scale horizontal heat transport, the synergies observed at S1 (0.35℃) and S2 (0.34℃) located in the northern was greater than that at S3 (0.31℃) and S4 (0.32℃) located in the southern city. From 11:00 BJT to 18:00 BJT, as the wind speed generally increased, the heat trapped within the urban area was effectively dissipated, resulting in a notable decline in synergistic effect at S3 and S4 in the southern part of the city. Due to the influence of heat transport, the decline in the synergistic effect was slower at stations located in the northern city. Taking the stations in the southern as examples, between 11:00 BJT and 18:00 BJT, the synergistic effect of S4 (composed of high-rise neighborhoods) was lower than that at S3 (composed of low-rise neighborhoods) by 0.01℃. This can be attributed to the shading provided by the high rise (Cai, 2017). As the solar altitude angle increases, the streets primarily receive energy from solar shortwave radiation, subsequently heating the air near the ground (Taleghani et al., 2016). Buildings of different heights block different amounts of solar shortwave radiation from reaching the ground (Zhang et al., 2016). Pavement and walls shaded by high-rise buildings lead to a decrease in air temperature (Krayenhoff & Voogt, 2016; Taleghani et al., 2016; Cai, 2017). From 19:00 BJT to 04:00 BJT the following day, the enhancement of high-rises on the local thermal environment became dominant, primarily due to their increased heat release, reduced heat loss from streets, and lower wind speeds. Notably, during this period, the synergistic effect observed at S4 exceeded that at S3 by 0.07℃. Consequently, during the valley breeze phase, large-scale horizontal heat transport contributed to significantly higher urban excess warming in the northern region compared to the southern. Furthermore, during the valley breeze phase, the vertical characteristics of urban morphology exert complex influences on the amplification of CHUII. While the increased heat release, reduced heat loss, and lower wind speeds associated with the high-rise street zone supported the amplification of CUHII, the shadowing effect of the high-rise street zone could constrain its amplification.

5 Conclusions

This study selected Beijing as the research subject, utilizing high-density AWS data from 2016 to 2020 as the research sample. Through remote sensing data and a machine learning model, the synergies between HW and CUHI in Beijing were analyzed.

In comparison to NHW wave periods, HW events significantly amplified the average daily CUHII, leading to an average increase of 59.33%. The maximum urban excess warming was observed between the Second and Fourth Rings of Beijing. The correlation coefficients between wind speed and amplified CUHII during mountain breeze periods and valley breeze periods were -0.11 and -0.27, respectively. On an urban scale, the large-scale horizontal heat transport caused by the turning mountain-valley breeze led to an asymmetric pattern of urban excess warming from north to south during heatwave periods. Furthermore, the effects of urban morphology on urban excess warming could not be overlooked. LCZ1 in the built-up area has the highest CUHII (1.71℃), followed by LCZ2 (1.43℃). Compared to the linear model and the SVR model, the RF model could be considered a reliable tool for fitting the relationship between amplified CHUII and urban morphology. The associations between 3D morphological indicators and CHUII difference were generally higher than those of 2D indicators. The SVF, which has the highest significance among all two-dimensional and three-dimensional indicators, exerts a dual influence on the amplified CHUII. During the mountain breeze phase, the amplification of CUHII in the high-rise street zone was more pronounced compared to that in the low-rise street zone. However, during the valley breeze phase, the high-rise street zone exhibited multiple impacts on the amplification of CHUII. In comparison to the low-rise street zone, the amplification of CUHII in the high-rise street zone was weaker in the afternoon but stronger at night.

In the future, we will continue to investigate into the mechanism of synergies between HW and CUHI using high-resolution observational data and numerical models, to provide crucial theoretical foundations and technological support for the construction of a comprehensive high-temperature monitoring, forecasting, and warning system.

Data availability. The hourly AWS observation data are available upon request from the China Meteorological Data Service Center (http://data.cma.cn/en). The land cover data are available at https://zenodo.org/record/5816591 (Yang & Huang, 2021).

Author contributions. Tao, S., Yuanjian, Y. and Gaopeng, L. conceptualized the study. Zuofang, Z. performed the model development, conducted the simulations. Tao, S. wrote the original manuscript and plotted all the figures. Yucheng, Z., Ye, T., Lei, L., and Simone, L. assisted in the conceptualization and model development. All the authors contributed to the manuscript preparation, discussion, and writing.

Financial support. This study was supported by the National Natural Science Foundation of China (42105147), the Joint Research Project for Meteorological Capacity Improvement (22NLTSQ013), and the Collaborative Innovation Fund of the Education Department of Anhui Province (GXXT-2023-050).

Competing interests. The contact author has declared that none of the authors has any competing interests.

https://doi.org/10.5194/egusphere-2024-1200
Preprint. Discussion started: 14 May 2024

References

Alonso, L., & Renard, F: A New Approach for Understanding Urban Microclimate by Integrating Complementary Predictors at Different Scales in Regression and Machine Learning Models. Remote Sensing, 12, 2434, https://doi.org/10.3390/rs12152434, 2020.

Ao, X., Wang, L., Zhi, X., Gu, W., Yang, H., Li, D.: Observed synergies between urban heat islands and heat waves and their controlling factors in Shanghai, China, J. Appl. Meteorol. Climatol., https://doi.org/10.1175/jamc-d-19-0073.1, 2019.

Bady M, Kato S, Takahashi T, Huang, H.: An experimental investigation of the wind environment and air quality within a densely populated urban street canyon, Journal of Wind Engineering and Industrial Aerodynamics, 99, 8, 857–867, https://doi.org/10.1016/j.jweia.2011.06.005, 2011.

Berger, C., Rosentreter, J., Voltersen, M., Baumgart, C., Schmullius, C., & Hese, S.: Spatio-temporal analysis of the relationship between 2D/3D urban site characteristics and land surface temperature, Remote Sensing of Environment, 193, 225–243, https://doi.org/10.1016/j.rse.2017.02.020, 2017.

Breiman L.: Random forest.Machine Learning, 45, 5–32, 2001.

Cai, H.: Impacts of built-up area expansion in 2D and 3D on regional surface temperature, Sustainability, https://doi.org/10.3390/su9101862, 2017.

Cao, J., Liu, X., Li, G., Zou, H.: Analysis of the phenomenon of Lake-land breeze in Poyang Lake area, Plateau Meteorol. Chin., 426–435, 10.7522/J.ISSN.1000-0534.2013.00197, 2015.

Chen, S., Yang, Y., Deng, F., Zhang, Y., Liu, D., Liu, C., Gao, Z.: A high-resolution monitoring approach of canopy urban heat island using a random forest model and multi-platform observations, Atmospheric Measurement Techniques, 15, 735–756, https://doi.org/10.5194/amt-15-735-2022, 2022.

Ding, Y.: Climate change and urbanization effects on extreme rainstorm in megacities of China, China Flood & Drought Management, 28, 2, 2, https://doi.org/CNKI:SUN:FHKH.0.2018-02-002, 2018.

Dou, J., Wang, Y., Miao, S.: Fine Spatial and Temporal Characteristics of Humidity and Wind in Beijing Urban Area. Journal of Applied Meteorological Science, 25, 5, 559–569, https://doi.org/10.11898/1001-7313.20140505, 2014.

Drach, P., Kru¨ger, E. L., Emmanuel, R.: Effects of atmospheric stability and urban morphology on daytime intra-urban temperature variability for Glasgow, UK. Sci. Total Environ., 627, 782–791, https://doi.org/10.1016/j.scitotenv.2018.01.285, 2018.

Du, J., Wang, K., Wang, J., & Ma, Q.: Contributions of surface solar radiation and precipitation to the spatiotemporal patterns of surface and air warming in China from 1960 to 2003. Atmospheric Chemistry and Physics, 17, 8, 4931–4944, https://doi.org/10.5194/acp-17-4931-2017, 2017.

Emmanuel, R., Rosenlund, H., Johansson, E.: Urban shading-a design option for the tropics? A study in Colombo, Sri Lanka, International Journal of Climatology, 27, 14, https://doi.org/10.1002/joc.1609, 2010.

Erell, E., Pearlmutter, D., & Williamson, T. J.: Urban Microclimate: Designing the Spaces between Buildings, London, New York, Routledge, 2011.

Fenner, D., Holtmann, A., Meier, F., Langer, I., Scherer, D.: Contrasting changes of urban heat island intensity during hot weather episodes, Environ. Res. Lett., 14, 12, 124013, https://doi.org/10.1088/1748-9326/ab506b, 2019.

Fenner, D., Meier, F., Bechtel, B., Otto, M., Scherer, D.: Intra and inter 'local climate zone' variability of air temperature as observed by crowdsourced citizen weather stations in Berlin, Germany, Meteorologische Zeitschrift, 26, 5, 525–547, https://doi.org/10.1127/metz/2017/0861, 2017.

Founda, D., Pierros, F., Petrakis, M., et al.: Interdecadal variations and trends of the urban heat island in Athens (Greece) and its response to heat waves. Atmospheric Research,161–162, 1–13, https://doi.org/10.1016/j.atmosres.2015.03.016, 2015.

Gao, J., Sun, Y., Liu, Q., Zhou, M., Lu, Y., & Li, L.: Impact of extreme high temperature on mortality and regional level definition of heat wave: A multi-city study in China, Science of the Total Environment, 505, 535–544, https://doi.org/10.1016/j.scitotenv.2014.10.028, 2015.

Gemechu, F. G.: How the interaction of heatwaves and urban heat islands amplify urban warming, Advances in Environment and Engineering Research, 3, 2, https://doi.org/10.21926/aeer.2202022, 2022.

Guo G, Zhou X, Wu Z, Xiao, R., Chen, Y.: Characterizing the impact of urban morphology heterogeneity on land surface temperature in Guangzhou, China, Environmental Modelling & Software, 84, 427–439, https://doi.org/10.1016/j.envsoft.2016.06.021, 2016.

Hang, J., Li, Y., Sandberg, M.: Experimental and numerical studies of flows through and within high-rise building arrays and their link to ventilation strategy. J Wind Eng Ind Aerodyn, 99, 1036–1055, https://doi.org/10.1016/j.envsoft.2016.06.021, 2011.

Hastie, T., Tibshirani, R. & Friedman, J.: The Elements of Statistical Learning: Data mining, Inference, and Prediction. 2nd Edition, Springer Series in Statistics, Springer, New York, 2009.

He B-J. Potentials of meteorological characteristics and synoptic conditions to mitigate urban heat island effects, Urban Climate, 24, 26–33, https://doi.org/10.1016/j.uclim.2018.01.004, 2018.

He, B. J., Wang, J., Liu, H., & Ulpiani, G.: Localized synergies between heat waves and urban heat islands: Implications on human thermal comfort and urban heat management. Environmental Research, 193, 110584, https://doi.org/10.1016/j.envres.2020.110584, 2021.

IPCC (Intergovernmental Panel on Climate Change). Climate Change 2013: ThePhysical Science Basis. Contribution of Working Group I to the Fifth Assessment Reportof the Intergovernmental Panel on Climate Change, Cambridge University Press, Cambridge and New York, 2013.

IPCC (Intergovernmental Panel on Climate Change). Climate Change 2021: ThePhysical Science Basis. Contribution of Working Group I to the Sixth Assessment Reportof the Intergovernmental Panel on Climate Change, Cambridge University Press,Cambridge and New York, 2021.

Jia, S., J., Wang, Y., Chen, L., & Bi, X.: A novel approach to estimating urban land surface temperature by the combination of geographically weighted regression and deep neural network models, Urban Climate, 47, 101390. https://doi.org/10.1016/j.uclim.2022.101390, 2023.

Jiang, S., Lee, X., Wang, J., Wang, K.: Amplified urban heat islands during heat wave periods, J. Geophys. Res. Atmos., 124, 14, 7797–7812, https://doi.org/10.1029/2018jd030230, 2019.

Khan, H. S., Paolini, R., Santamouris, M., Caccetta, P.: Exploring the synergies between urban overheating and heatwaves (HWs) in Western Sydney, Energies, 13, 2, 470, https://doi.org/10.3390/en13020470, 2020.

Li, D., Bou-Zeid, E.: Synergistic Interactions between Urban Heat Islands and Heat Waves: The Impact in Cities Is Larger than the Sum of Its Parts, Journal of Applied Meteorology and Climatology, 52, 9, 2051–2064, https://doi.org/10.1175/JAMC-D-13-02.1, 2013.

Li Q.: Statistical modeling experiment of land precipitation variations since the start of the 20th century with external forcing factors. Chinese Science Bulletin, 65, 21, 2266–2278, https://doi.org/10.1360/TB-2020-0305, 2020.

Liu, S., Liu, Z., Li, J., Wang, Y,; Ma, Y., Sheng, L., Liu, H., Liang, F., Xin, G., Wang, J.: Numerical simulation for the coupling effect of local atmospheric circulations over the area of Beijing, Tianjin and Hebei Province, Science in China (Series D: Earth Sciences), 3, 11, https://doi.org/10.1007/s11430-009-0030-2, 2009.

Liu, W., Ji, C., Zhong, J., Jiang, X., and Zheng, Z. Temporal characteristics of the Beijing urban heat island, Theor. Appl. Climatol., 87, 1–4, 213–221, https://doi.org/10.1007/s00704-005-0192-6, 2007.

Merckx, T., Souffreau, C., Kaiser, A., Baardsen, L. F., Backeljau, T.,; Bonte, D., Brans, K. I., Cours, M., Dahirel, M., Debortoli, N., et al.: Body-size shifts in aquatic and terrestrial urban communities, Nature, 558, 7708, https://doi.org/10.1038/s41586-018-0140-0, 2018.

Miao, Y., Liu, S., Chen, B., Zhang, B., Wang, S., Li, S.: Simulating urban flow and dispersion in Beijing by coupling a CFD model with the WRF model, Advances in Atmospheric Sciences, 30, 6, 1663-1678, https://doi.org/10.1007/s00376-013-2234-9, 2013.

Ng, E.: Policies and technical guidelines for urban planning of high-density cities-air ventilation assessment (AVA) of Hong Kong. Building and Environment, 44, 7, 1478–1488, https://doi.org/10.1016/j.buildenv.2008.06.013, 2009.

Ngarambe, J., Nganyiyimana, J., Kim, I., Santamouris, M., Yun, G. Y.: Synergies between urban heat island and heat waves in Seoul: The role of wind speed and land use characteristics. PLoS ONE, 15, 12, https://doi.org/10.1371/journal.pone.0243571, 2020.

Oke, T.R., Mills, G., Christen, A., Voogt, J. A.: Urban Climates, Cambridge University Press, 2017.

Patz, J. A., Campbell-Lendrum, D., Holloway, T., and Foley, J. A. Impact of regional climate change on human health, Nature, 438, 310–317, https://doi.org/10.1038/nature04188, 2017.

Peng, F., Wong M. S., Ho, H. C., Nichol, J., Chan, P. W.: Reconstruction of historical datasets for analyzing spatiotemporal influence of built environment on urban microclimates across a compact city. Build. Environ., 123, 649–660, https://doi.org/10.1016/j.buildenv.2017.07.038, 2017.

https://doi.org/10.5194/egusphere-2024-1200
Preprint. Discussion started: 14 May 2024

Perini, K., Magliocco, A.: Effects of vegetation, urban density, building height, and atmospheric conditions on local temperatures and thermal comfort. Urban Forestry & Urban Greening, 13, 3, 495–506, https://doi.org/10.1016/j.ufug.2014.03.003, 2014.

Rafiee, A., Dias, E., Koomen, E.: Urban forestry & urban greening Local impact of tree volume on nocturnal urban heat island: a case study in Amsterdam, Urban For Urban Green, 16, 50–61, https://doi.org/10.1016/j.ufug.2016.01.008, 2016.

Ren, G., Chu, Z., Chen, Z., Ren, Y.: Implications of temporal change in urban heat island intensity observed at Beijing and Wuhan stations, Geophysical Research Letters, 34, 5, https://doi.org/10.1029/2006GL027927, 2007.

Russo, S., Dosio, A., Graversen, R. G., Sillmann, J., Carrao, H., Dunbar, M. B., Singleton, A., Montagna, P., Barbola, P., Vogt, J. V.: Magnitude of extreme heat waves in present climate and their projection in a warming world, Journal of Geophysical Research: Atmospheres, l, 19, 22, 500–512, https://doi.org/10.1002/2014JD022098, 2014.

Ryu, Y. H., Baik, J. J.: Quantitative analysis of factors contributing to urban heat island intensity. J. Appl. Meteorol. Climatol., 51, 5, 842–854, https://doi.org/10.1175/JAMC-D-11-098.1, 2012.

Scarano, M., Mancini, F. Assessing the relationship between sky view factor and land surface temperature to the spatial resolution. Int. J. Remote Sens., 38, 6910–6929, https://doi.org/10.1080/01431161.2017.1368099, 2017.

Krayenhoff, E. S., Voogt, J. A.: Daytime thermal anisotropy of urban neighbourhoods: morphological causation, Remote Sens., 8, 2, https://doi.org/10.3390/rs8020108, 2016.

Seto, K. C., Guneralp, B., Hutyra, L. R.: Global forecasts of urban expansion to 2030 and direct impacts on biodiversity and carbon pools. Proceedings of the National Academy of Sciences, 109, 40, 16083–16088, https://doi.org/10.1073/pnas.1211658109, 2012.

Shi, T., Huang, Y., Shi, C., & Yang, Y.: Influence of Urbanization on the Thermal Environment of Meteorological Stations: Satellite-observational Evidence, Advances in Climate Change Research, 1, 7–15, https://doi.org/10.1016/j.accre.2015.07.001, 2015.

Smola, A. J., & Schölkopf, B.: A tutorial on support vector regression, Statistics and computing, 14, 3, 199–222, https://doi.org/10.1023/B:STCO.0000035301.49549.88, 2004.

Srivanit, M., Kazunori, H.: The influence of urban morphology indicators on summer diurnal range of urban climate in Bangkok metropolitan area, Thailand, International Journal of Civil & Environmental Engineering, 11, 5, 34–46, 2011.

Stewart, I. D., Oke, T. R., Krayenhoff, E. S.: Evaluation of the 'local climate zone' scheme using temperature observations and model simulations, International Journal of Climatology, 34, 4, 1062–1080, https://doi.org/10.1002/joc.3746, 2014.

Stewart, I. D., & Oke T. R. Local climate zones for urban temperature studies, Bulletin of the American Meteorological Society, 93, 12, 1879–1900. https://doi.org/10.1175/BAMS-D-11-00019.1, 2012.

Sun, J., Wang, H., Yuan, W.: Decadal variability of the extreme hot event in China and its association with atmospheric circulations. Climatic and Environmental Research, 16, 2, 199–208, 2011.

https://doi.org/10.5194/egusphere-2024-1200
Preprint. Discussion started: 14 May 2024

Taleghani, M., Sailor, D., Ban-Weiss, G. A.: Micrometeorological simulations to predict the impacts of heat mitigation strategies on pedestrian thermal comfort in a Los Angeles neighborhood. Environ. Res. Lett., 11, 2, https://doi.org/10.1088/1748-9326/11/2/024003, 2016.

Tan, M., Liu, K., Liu, L.,Zhu, Y., & Wang, D.: Population Spatialization of 30 m Grid in Pearl River Delta Based on Stochastic Forest Model. Progress in Geography, 36, 10, 122-130. https://doi.org/10.18306/dlkxjz.2017.10.012, 2017

Tian, Y., Miao, J.: Overview of Mountain-Valley Breeze Studies in China. Meteorological Science and Technology, 47, 1, 11. https://doi.org/10.19517/j.1671-6345.20170777, 2019.

Tian, Y., Zhou, W., Qian, Y., Zheng, Z., Yan, J.: The effect of urban 2D and 3D morphology on air temperature in residential neighborhoods, Landscape Ecology, 34, 5, 1161–1178, https://doi.org/10.1007/s10980-019-00834-7, 2019.

Tompalski, P., & Wężyk, P.: LiDAR and VHRS Data for Assessing living quality in cities—an approach based on 3D spatial indices, International Archives of the Photogrammetry, Remote Sensing and Spatial Information Sciences, https://doi.org/10.5194/isprsarchivesXXXIX-B6-173-2012, 2012.

Unger J.: Intra-urban relationship between surface geometry and urban heat island: review and new approach. Clim. Res., 27, 253–264, https://doi.org/10.3354/cr0272532004.

Unger, J., Sümeghy, Z., Zoboki, J.: Temperature cross-section features in an urban area, Atmospheric Research, 58, 2, 117–127, https://doi.org/10.1016/S0169-8095(01)00087-4, 2001.

Walsh, J. E., & Chapman, W. L.: Arctic cloud-radiation-temperature associations in observational data and atmospheric reanalyses, Journal of Climate, 11, 11, 3030–3045, https://doi.org/10.1175/1520-0442(1998)0112.0.CO;2, 1998.

Wang, Y., Zheng, D., Li, Q.: Urban meteorological disasters. Beijing: China Meteorological Press, 2009.

Wei, J., Sun, J.: The analysis of summer heat wave and sultry weather in North China, Climatic and Environmental Research, 12, 3, 453–463, https://doi.org/10.1175/1520-0442(1998)011<3030:acrtai>2.0.co;2, 2007.

Xie, J., Sun, T., Liu, C., Li, L., Xu, X., Miao, S., Lin, L., Chen, Y., Fan, S.: Quantitative evaluation of impacts of the steadiness and duration of urban surface wind patterns on air quality, Sci. Total Environ., 850, https://doi.org/10.1016/j.scitotenv.2022.157957, 2022.

Xu, W. H., Li, Q. X., Wang, X. L., Yang, S., Cao, L., Feng, Y.: Homogenization of Chinese daily surface air temperatures and analysis of trends in the extreme temperature indices, Journal of Geophysical Research-Atmospheres, 118, 17, 9708–9720, https://doi.org/10.1002/jgrd.50791 , 2013.

Xu, Z., Fitzgerald, G., Guo, Y., Jalaludin, B., Tong, S.: Impact of heatwave on mortality under different heatwave definitions: A systematic review and meta-analysis, Environ. Int., 89–90, 193-203. https://doi.org/10.1016/j.envint.2016.02.007, 2016.

Xue, J., Zong, L., Yang ,Y., Bi, X., Zhang, Y., Zhao, M.: Diurnal and interannual variations of canopy urban heat island (CUHI) effects over a mountain-valley city with a semi-arid climate, Urban Climate, 48, https://doi.org/10.1016/j.uclim.2023.101425, 2003.

https://doi.org/10.5194/egusphere-2024-1200
Preprint. Discussion started: 14 May 2024

Yang, J., Su, J., Xia, J., Jin, C., Li, X., Ge, Q.: The Impact of Spatial Form of Urban Architecture on the Urban Thermal Environment: A Case Study of the Zhongshan District, Dalian, China, IEEE Journal of Selected Topics in Applied Earth Observations and Remote Sensing, 11, 8, 2709–2716, https://doi.org/10.1109/JSTARS.2018.2808469, 2018.

Yang, J., Huang, X.: The 30 m annual land cover dataset and its dynamics in China from 1990 to 2019. Earth System Science Data, 13, 8, 3907–3925. https://doi.org/10.5194/essd-13-3907-2021, 2021.

Yang, P., Liu, W.D., Zhong, J.Q., Yang, J. Evaluating the Quality of Temperature Measured at Automatic Weather Stations in Beijing, Journal of Applied Meteorological Science, 22, 6, 706–715, https://doi.org/1001-7313(2011)22:6<706:BJDQZD>2.0.TX;2-2 , 2011.

Yang, Y., Guo, M., Wang, L., Zong, L., Liu, D., Zhang, W., Wang, M., Wan, B., Guo, Y.: Unevenly spatiotemporal distribution of urban excess warming in coastal Shanghai megacity, China: Roles of geophysical environment, ventilation and sea breeze, Building and Environment, 235, https://doi.org/10.1016/j.buildenv.2023.110180, 2023.

Yang, Y., Zheng, X., Gao, Z., Wang, H., Wang, T., Li, Y., Lau, G. N. C., Yim, S. H. L. Long-Term Trends of Persistent Synoptic Circulation Events in Planetary Boundary Layer and Their Relationships With Haze Pollution in Winter Half Year Over Eastern China, J. Geophys. Res.-Atmos., 123, 10991–11007. https://doi.org/10.1029/2018JD028982, 2018.

Yang, Y., Zheng, Z., Yim, S. Y. L., Roth, M., Ren, G., Gao, Z., Wang, T., Li, Q., Shi, C., Ning, G. PM 2.5 Pollution Modulates Wintertime Urban Heat Island Intensity in the BeijingTianjin-Hebei Megalopolis, China, Geophys. Res. Lett., 47, 1, 1–12, https://doi.org/10.1029/2019GL084288, 2020.

Yu, Z., Chen, S., Wong, N., Ignatius, M., Deng, J., He, Y., & Hii, D. J. C. Dependence between urban morphology and outdoor air temperature: A tropical campus study using random forests algorithm, Sustainable Cities and Society, 61, 1, 1–12, https://doi.org/10.1016/j.scs.2020.102200, 2020.

Zakšek, K., Oštir, K., Kokalj, Ž.: Sky-view factor as a relief visualization technique, Remote Sens, https://doi.org/10. 3390/rs3020398, 2011.

Zhang, H., Zhu, S., Gao, Y., Zhang, G.: The Relationship Between Urban Spatial Morphology Parameters and Urban Heat Island Intensity Under Fine Weather Condition. Journal of Applied Meteorological Science, 27, 2, 249–256. https://doi.org/10.11898/1001-7313.20160213, 2016.

Zhang, N., Zhu, L. F., Zhu, Y. Urban heat island and boundary layer structures under hot weather synoptic conditions: a case study of Suzhou City, China, Advances in Atmospheric Sciences, 28, 4, 855–865, https://doi.org/10.1007/s00376-010-0040-1, 2011.

Zheng, Z., Ren, G., Gao, H., Yang, Y.: Urban ventilation planning and its associated benefits based on numerical experiments: A case study in beijing, China, Building and Environment, 109383, https://doi.org/10.1016/j.buildenv.2022.109383, 2022.

Zheng, Z., Ren, G., Wang, H., Dou, J., Gao, Z., Duan, C., Li, Y., Ngarukiyimana, J. P., Zhao, C., Cao, C., et al.: Relationship between fine-particle pollution and the urban heat island in Beijing, China: Observational evidence. Boundary-layer Meteorology, 169, 93–113, https://doi.org/10.1007/s10546-018-0362-6, 2018.

Zheng, Z., Zhao, C., Lolli, S., Wang, X., Wang, Y., Ma, X., Li, Q., Yang, Y.: Diurnal variation of summer precipitation modulated by air pollution: Observational evidences in the Beijing metropolitan area, Environ. Res. Lett., 15, 094053, https://doi.org/10.1088/1748-9326/ab99fc, 2020.

Zheng, Z., Ren, G., Gao, H. Analysis of the local circulation in Beijing area, Meteorological Monthly, 44, 3, 425–433, https://doi.org/10.7519/j.issn.1000-0526.2018.03.009, 2018.

Zhou, D., Zhao, S., Liu, S., Zhang, L., Zhu, C.: Surface urban heat island in China's 32 major cities: Spatial patterns and drivers. Remote Sensing of Environment, 152, 51–61, https://doi.org/10.1016/j.rse.2014.05.017, 2014.

Zhou, X., Okaze, T., Ren, C., Cai, M., Mochida, A.: Evaluation of urban heat islands using local climate zones under the influences of sea-Land breeze, Sustainable Cities and Society, 55, 102060, https://doi.org/10.1016/j. scs.2020.102060, 2020.

Zinzi, M., Agnoli, S., Burattini, C., Mattoni, B.: On the thermal response of buildings under the synergic effect of heat waves and urban heat island, Solar Energy, 211, 10, 1270–1282, https://doi.org/10.1016/j.solener.2020.10.050, 2020.

Zong, L., Liu, S., Yang, Y., Ren, G., Yu, M., Zhang, Y., Li, Y. Synergistic Influence of Local Climate Zones and Wind Speeds on the Urban Heat Island and Heat Waves in the Megacity of Beijing, China, Front. Earth Sci., 9, 673786, https://doi.org/10.3389/feart.2021.673786, 2021.

Zong, L., Yang, Y., Xia, H., Gao, M., Sun, Z., Zheng, Z., Li, X., Ning, G., Li, Y., Lolli, S.: Joint occurrence of heatwaves and ozone pollution and increased health risks in Beijing, China: roles of synoptic weather pattern and urbanization, Atmos. Chem. Phys, 22, 10, 6523–6538, https://doi.org/10.5194/acp-22-6523-202, 2022.

Figures S1 and S2